This is the peer-reviewed, final accepted version for American Mineralogist, published by the Mineralogical Society of America.
The published version is subject to change. Cite as Authors (Year) Title. American Mineralogist, in press.
DOI: https://doi.org/10.2138/am-2021-7784. http://www.minsocam.org/

REVISION 1

Various antiphase domains in garnet-hosted omphacite in low temperature eclogite: A FIB–TEM study on heterogeneous ordering processes

Ryo Fukushima[1], Tatsuki Tsujimori[1,2], Nobuyoshi Miyajima[3]

[1] Graduate School of Science, Tohoku University, Sendai 980-8578, Japan

[2] Center for Northeast Asian Studies, Tohoku University, Sendai 980-8576, Japan

[3] Bayerisches Geoinstitut, Universität Bayreuth, 95440 Bayreuth, Germany

Running title: Antiphase domains in garnet-hosted omphacite

Corresponding author: Ryo Fukushima

E-mail address: ryo.fukushima.p7@dc.tohoku.ac.jp

Address: Graduate School of Science, Tohoku University, 41 Kawauchi, Aoba, Sendai 980-8578, Japan

Phone/Fax: +81-22-795-6236

Always consult and cite the final, published document. See http:/www.minsocam.org or GeoscienceWorld

This is the peer-reviewed, final accepted version for American Mineralogist, published by the Mineralogical Society of America.
The published version is subject to change. Cite as Authors (Year) Title. American Mineralogist, in press.
DOI: https://doi.org/10.2138/am-2021-7784. http://www.minsocam.org/

ABSTRACT

Low-temperature omphacite has peculiar microstructures called 'antiphase domains (APDs)', which can be formed via phase transition from disordered *C*2/*c* to ordered *P*2/*n* structure during cooling. Hence morphological analyses of the APDs of undeformed omphacite have a potential to unravel the temperature–time (*T*–*t*) histories of the eclogite. We investigated five omphacite inclusions in a euhedral garnet porphyroblast obtained from low-temperature eclogite in Syros. The garnet (~6 mm in size) exhibits a distinct prograde chemical zoning and contains abundant mineral inclusions. Transmission electron microscope (TEM) observations of the focused ion beam (FIB) foils confirmed a heterogeneous distribution of equiaxed APDs (10–280 nm in diameter) and columnar APDs. Size distributions of the equiaxed APDs are characterized by kurtosis values of −0.45–3.91, which are larger than those in the matrix omphacite. The columnar APDs are subdivided into two types: dislocation-related (Type I) and inclusion–host interfacial (Type II). The presence of Type I APDs suggests the inclusions were deformed prior to the host garnet growth. In contrast, Type II APDs, which are characterized by a bundle of stripe-like APDs (~40 nm in width) aligned perpendicular to the host garnet, imply the simultaneous growth of omphacite and garnet in a non-deformation state. The presence of these two contrasting APDs of omphacite inclusions in the single prograde-zoned garnet prevents a simple application of geospeedometry based on APD sizes. Nevertheless, our observations demonstrate that APDs are keys to understanding thermodynamic equilibrium states and the mineral growth kinetics during eclogitization.

Keywords

omphacite, antiphase domain (APD), garnet, transmission electron microscopy (TEM), eclogite

Always consult and cite the final, published document. See http:/www.minsocam.org or GeoscienceWorld

This is the peer-reviewed, final accepted version for American Mineralogist, published by the Mineralogical Society of America.
The published version is subject to change. Cite as Authors (Year) Title. American Mineralogist, in press.
DOI: https://doi.org/10.2138/am-2021-7784. http://www.minsocam.org/

INTRODUCTION

Omphacite, clinopyroxene with a composition close to $Ca_{0.5}Na_{0.5}[Mg,Fe^{2+}]_{0.5}Al_{0.5}Si_2O_6$, is one of the prominent minerals which, together with garnet, compose eclogite (cf. Tsujimori and Mattinson, 2020). It occurs ubiquitously in a variety of high-pressure (H*P*) and ultrahigh-pressure (UH*P*) metamorphic rocks, typically in basaltic protoliths. Its parageneses and major-element compositions have been commonly used to characterize subducted oceanic-crusts in the H*P*–UH*P* metamorphic belts. Omphacite at high temperature has a cation-disordered structure with *C*2/*c* symmetry (e.g., Warner 1964; Clark et al. 1969). At temperatures recorded in blueschist and most orogenic eclogites, however, the difference in space-group symmetry between ordered *P*2/*n* omphacite and disordered *C*2/*c* diopsidic pyroxene allows miscibility regions between jadeitic pyroxene (*C*2/*c*)–omphacite (*P*2/*n*) and augitic pyroxene (*C*2/*c*)–omphacite (*P*2/*n*) (e.g., Matsumoto and Banno 1970; Yokoyama et al. 1976; Carpenter 1979a, 1980; Tsujimori 1997; Tsujimori and Liou 2004; Tsujimori et al. 2005; García-Casco et al. 2009; Takahashi et al. 2017).

Cation ordering in omphacite has been investigated in numerous transmission electron microscopic (TEM) studies; the cation ordering forms characteristic bubble-like or column-like microstructures, called 'antiphase domains (APDs)'. If disordered omphacite is cooled down to some extent, multiple ordered phases nucleate and pin each other because of discrepancies in cation positions at their boundaries. These boundaries are commonly called 'antiphase domain boundaries (APDBs)', and can be observed under TEM. It is considered that APDBs can be formed just if omphacite crystallizes in the *P*2/*n* stable field, as many researchers think that the nucleation of the disordered phase predates APDBs formation (e.g., Champness 1973; Carpenter 1978).

Always consult and cite the final, published document. See http:/www.minsocam.org or GeoscienceWorld

This is the peer-reviewed, final accepted version for American Mineralogist, published by the Mineralogical Society of America.
The published version is subject to change. Cite as Authors (Year) Title. American Mineralogist, in press.
DOI: https://doi.org/10.2138/am-2021-7784. http://www.minsocam.org/

An averaged diameter of equiaxed APDs (δ) can be calculated with the following equation (Carpenter 1981):

$$\delta^8 = 8 \times 6 \times 10^{35} \exp\left(-\frac{75000}{RT}\right) t$$

where t is annealing time and T is temperature. This function involving t and T would allow for geothermometry and/or geospeedometry and lead to a deeper understanding of the kinetics of low-T eclogitization of a subducting slab. However, the application of this equation to natural omphacites is not that simple because omphacite-bearing blueschists and orogenic eclogites have commonly undergone deformation and because the original APDBs would have been modified very easily (Van Roermund and Lardeaux 1991). Brenker et al. (2003) suggested a potential approach to exclude deformational modifications of original APDs. Specifically, they postulated that garnets could act as rigid capsules that prevent the dynamic recrystallization of omphacite inclusions. Nevertheless, no one has attempted to challenge the approach yet. Thus, in this study, we conducted a transmission electron microscopic (TEM) study combined with focused ion beam (FIB) technique on omphacite inclusions within a prograde-zoned garnet. The aim of our reconnaissance is to contribute to the understanding of the growth kinetics of omphacite inclusions within garnet porphyroblasts, as well as the low-T eclogitization of a subducting slab.

SAMPLE DESCRIPTION

We examined a euhedral garnet porphyroblast (~6 mm in size) extracted from a low-T eclogite of the Cycladic Blueschist Unit (CBU), Syros, Greece (Fig. 1). The garnet exhibits a rhombic dodecahedron shape with twelve crystallographic equivalent {110} planes.

Syros Island, which belongs to Cyclades Archipelago, is located at the center of the Aegean domain. The metamorphic sequence consists mainly of alternating marbles and H*P*

Always consult and cite the final, published document. See http:/www.minsocam.org or GeoscienceWorld

This is the peer-reviewed, final accepted version for American Mineralogist, published by the Mineralogical Society of America.
The published version is subject to change. Cite as Authors (Year) Title. American Mineralogist, in press.
DOI: https://doi.org/10.2138/am-2021-7784. http://www.minsocam.org/

schists. The CBU of Syros contains dismembered meta-ophiolite, whose protoliths were derived from hydrothermally-altered oceanic crust (Seck et al. 1996). The Cyclades Archipelago is the deepest exhumed parts of the belt and its peak-pressure conditions were achieved at ~53–48 Ma (Lagos et al. 2007; Lister and Forster 2016; Tomaschek et al. 2003; Uunk et al. 2018). The peak metamorphic condition of the CBU on Syros was estimated as T ~500–560°C and P ~2.2–2.4 GPa (Laurent et al. 2018), while Schumacher et al. (2008) suggested a lower condition at T ~500°C and P ~1.5–1.6 GPa.

ANALYTICAL PROCEDURES

SEM observation and EPMA X-ray mapping

To characterize the core-to-rim compositional zoning of the porphyroblastic garnet, we firstly cut the extracted garnet at nearly the center. Then, one of the center-cut garnets was mounted with epoxy resin and polished. The polished sample was observed using a JEOL JSM-7001F field emission-scanning electron microscope (FE-SEM) at Tohoku University. The back-scattered electron (BSE) imaging was performed at an acceleration voltage of 15 kV and a beam current of 3 nA. We identified mineral inclusions using a Hitachi S-3400N scanning electron microprobe (SEM) equipped with an Oxford INCA X-act energy dispersive X-ray (EDS) system at Tohoku University. The acceleration voltage and the beam current during the SEM-EDS observations were maintained at 15 kV and 1 nA, respectively. X-ray mapping (Mg, Ca, Fe and Mn) of the mounted garnet was performed by a JEOL JXA-8200 electron microprobe analyzer at Bayerishes Geoinstitut (BGI), at an acceleration voltage of 15 kV and a probe current of 500 nA.

FIB fabrication of omphacite

Always consult and cite the final, published document. See http:/www.minsocam.org or GeoscienceWorld

This is the peer-reviewed, final accepted version for American Mineralogist, published by the Mineralogical Society of America.
The published version is subject to change. Cite as Authors (Year) Title. American Mineralogist, in press.
DOI: https://doi.org/10.2138/am-2021-7784. http://www.minsocam.org/

A focused ion-beam (FIB) technique was used to extract foils of the omphacite inclusions in the garnet, using a FEI Scios DualBeam system equipped with a gallium (Ga) ion-gun for sample fabrication at BGI. Fabrication of thin foils (~100 nm in thickness) was done for the five omphacite inclusions [1C (core), 2M (mantle), 3R, 4R, 5R (rim)] in the order from the core to the rim of the garnet; for comparison, one foil (MX) was also extracted from a matrix-forming omphacite from the same eclogite. Note that we define two boundaries: one between the core and the mantle at 30% of the total radius from the center of crystal, and the other between the mantle and the rim at 85% (Fig. 2). These boundaries respectively correspond to the portion where the Y concentration peaks and the portion marking the beginning of Y–Mn enrichments (Fukushima et al. in revision). The locations of each inclusion can therefore be expressed as ~14% (1C), ~48% (2M), ~90% (3R), ~95% (4R), and ~98% (5R). The locations and morphology of the inclusions are shown in Figures 1 and 3.

TEM observation

The thin foil specimens of the omphacite inclusions were observed using a FEI Titan G2 80-200 S/TEM system at BGI. The microstructures of the omphacite were studied under conventional bright-field and dark-field TEM imaging modes and selected area electron diffraction. In addition, EDS X-ray mapping of major elements by scanning transmission electron microscopy (STEM), operated at a 200 kV acceleration voltage, was performed using four Silicon Drift Detector (SDD) detectors. The STEM-EDS maps were generated by scanning a focused beam with a diameter of about 0.2 nm and a dwell time of 16 microseconds across the samples.

Measurement of antiphase domain (APD) sizes

Always consult and cite the final, published document. See http:/www.minsocam.org or GeoscienceWorld

This is the peer-reviewed, final accepted version for American Mineralogist, published by the Mineralogical Society of America.
The published version is subject to change. Cite as Authors (Year) Title. American Mineralogist, in press.
DOI: https://doi.org/10.2138/am-2021-7784. http://www.minsocam.org/

To measure APD sizes, we processed the acquired digital images using an approach of the Trainable Weka Segmentation (Arganda-Carreras et al. 2017) bundled in an image processing package Fiji (Schindelin et al. 2012), which is a modified version of the open source, Java-based image processing program Image J (Abràmoff et al. 2004). This application enables us to divide an image with complicated patterns into two or more groups based on its color distribution. In each dark-field image, we chose certain areas where many distinct APDs were observed to binarize them. Here, the binarized image reflects the difference in brightness between the ordered and disordered domains. Then, we excluded APDs with abnormal shapes by setting a threshold of circularity (= $4\pi \times$ area / circumference^2). We also excluded some of the noise by setting a minimum APD size. Finally, we calculated the diameters of the APDs based on their areas, under the assumption that all of the measured APDs are circles.

In order to evaluate the reliability of this measurement protocol, in addition to our specimens, we also measured equiaxed APD sizes in a previously reported matrix-forming omphacite. Specifically, we processed the dark-field image (a scanned image from the literature) of sample #97647 in Carpenter (1978) (Fig. 2a in the literature) to measure its APD sizes.

MINERAL INCLUSIONS IN THE ZONED GARNET

The investigated garnet crystal (Fig. 1) contains abundant mineral inclusions (typically ~10–100 μm in size), mainly of omphacite (~40–50 mol% jadeite) and clinozoisite [$Fe^{3+}/(Fe^{3+} + Al)$ atomic ratio = ~0.2]. Omphacite occurs as irregularly rounded anhedral crystals with curved interfaces. The garnet crystal also contains minor amounts of rutile, titanite, carbonate, apatite, chlorite, quartz, paragonite, albite, jadeite (~95 mol% jadeite) and zircon. Titanite tends to occur

Always consult and cite the final, published document. See http:/www.minsocam.org or GeoscienceWorld

This is the peer-reviewed, final accepted version for American Mineralogist, published by the Mineralogical Society of America.
The published version is subject to change. Cite as Authors (Year) Title. American Mineralogist, in press.
DOI: https://doi.org/10.2138/am-2021-7784. http://www.minsocam.org/

at the core. Chlorite and albite are found as secondary replacements of primary inclusions along micro cracks.

Major-element EPMA X-ray maps of the garnet (5–9 mol% pyrope; 61–67% almandine; 1–3 spessartine; 24–30% grossular) are shown in Figure 1. The maps exhibit a concentric zoning pattern, where Mg# = Mg/(Mg + Fe^{2+}) roughly increases rimward and Mn decreases from the core to the mantle. Subtle Mn enrichments are found at the rim.

ANTIPHASE DOMAINS OF OMPHACITE

APD morphology and size distributions

TEM images of the omphacite inclusions are shown in Figures 4–6. Based on the morphology, the observed APDs are divided into two types: 1) equiaxed APDs and 2) columnar APDs. These two types frequently occur within a few μm squared areas, and the boundaries among two types are not clear. The columnar APDs, with stripe-like shapes, are further subdivided into two types. Type I columnar APDs occur as extensions from dislocations. In contrast, Type II columnar APDs are found at garnet–omphacite interfaces and exhibit regular-alignment perpendicular to the interfaces. Note that, unless aligned periodically, dislocation-related columnar APDs attached perpendicularly to garnet–omphacite interfaces are classified as Type I columnar APDs.

We found equiaxed APDs in all of the FIB foils including omphacite in the eclogitic matrix, although they were less abundant in the 2M and 4R. Type I columnar APDs, most of which were highly curved, were also common in the omphacite inclusions. Type II columnar APDs were found only in 1C and 3R. Since the morphology of such columnar APDs is somewhat complicated, it is difficult to measure their widths. Therefore, we only measured equiaxed APD sizes here.

Always consult and cite the final, published document. See http:/www.minsocam.org or GeoscienceWorld

This is the peer-reviewed, final accepted version for American Mineralogist, published by the Mineralogical Society of America.
The published version is subject to change. Cite as Authors (Year) Title. American Mineralogist, in press.
DOI: https://doi.org/10.2138/am-2021-7784. http://www.minsocam.org/

APD size variations are shown by histograms with the kernel density estimate in Figures 7 and 8. Measured data are presented in supplementary Table S1. Major modes are: ~40 nm (1C), ~30 nm (3R), ~20 nm (4R), ~60 nm (5R), ~60 nm (MX) and ~16 nm (#97647). Mean values are: 62 nm (1C), 67 nm (3R), 25 nm (4R), 98 nm (5R), 88 nm (MX) and 31 nm (#97647). In addition, we calculated skewness and kurtosis values to characterize the distributions. We adopted the definitions of b_1 (skewness) and b_2 (kurtosis) as set forth in Joanes and Gill (1998). Skewness values are: 1.53 (1C), 0.64 (3R), 1.91 (4R), 0.77 (5R), 0.48 (MX) and 0.56 (#97647). Kurtosis values are: 3.14 (1C), –0.45 (3R), 3.91 (4R), 0.02 (5R), –0.85 (MX) and –0.65 (#97647). All of the APD size distributions are non-Gaussian and seem to be expressed by slightly multi-modal distributions. For each, the secondary or higher-order modes are larger than the major mode thereof, and the mean value is larger than the major mode by 5–38 nm. The mean equiaxed APD size of #97647 (Carpenter 1978) is consistent with the reported value of 20–50 nm. However, our reassessment also confirmed an abundance of APDs smaller than 20 nm.

Peculiar features of individual APDs

Omphacite extracted from the garnet core (1C). 1C was extracted from the core of the garnet. Some regions of 1C (Fig. 4a) have both equiaxed APDs and Type II columnar APDs (width 20–130 nm, length ~130 nm). The widths of the Type II columnar APDs in 1C are not highly homogeneous (see supplementary Table S1 and Document S1). The other regions, however, show abundant Type I columnar APDs (Fig. 4b). They seem to have highly interacted with dislocations in the omphacite. Although they are also roughly perpendicular to the garnet–omphacite interface, they are not periodic.

Always consult and cite the final, published document. See http:/www.minsocam.org or GeoscienceWorld

This is the peer-reviewed, final accepted version for American Mineralogist, published by the Mineralogical Society of America.
The published version is subject to change. Cite as Authors (Year) Title. American Mineralogist, in press.
DOI: https://doi.org/10.2138/am-2021-7784. http://www.minsocam.org/

Omphacite extracted from the mantle of the garnet (2M). 2M was extracted from the mantle of the garnet. 2M (Fig. 5a) has mainly Type I columnar APDs and rare equiaxed APDs. Although these Type I columnar APDs are roughly perpendicular to the garnet–omphacite interface, they are not periodic.

Omphacites extracted from the garnet rim (3R, 4R and 5R). 3R, 4R and 5R were extracted from the rim of the garnet. 4R contains mainly Type I columnar APDs (Figs. 6a–d), while 3R (Figs. 5b and 5c) and 5R (Fig. 6e) have mainly equiaxed APDs. Equiaxed APDs were minor in 4R. The samples also showed differences with regards to APD shapes near the garnet–omphacite grain interfaces. In 4R, some Type I columnar APDs are attached perpendicularly to the garnet–omphacite interface (Fig. 6b), but the other regions never exhibit such textures (Fig. 6c). In the latter case, we observed fracture-like pores (~50 nm in width; Fig. 6d). In contrast, 5R does not contain Type I columnar APDs (Fig. 6e). 3R is similar to 5R in that both have abundant equiaxed APDs (Fig. 5b), but it is significantly different in the regions relatively close to the garnet core. Specifically, 3R encompasses Type II columnar APDs (Fig. 5c), which are characterized by a bundle of elongated APDs aligned perpendicular to the garnet–omphacite interface. All of them are perpendicular to the interface and have a moderately homogenous width of 38 ± 11 nm (n = 19, 1σ) and length of ~130 nm (see supplementary Table S1 and Document S1). Although Type II columnar APDs were also observed in 1C, their widths are not highly homogeneous like in 3R. This peculiar texture was investigated by STEM-EDS X-ray mapping of Na, Ca, and Fe (Fig. 9). The Na- and Ca- distributions are homogenous throughout the specimen, while the Fe concentration is slightly lower at the omphacite rim that has the Type

Always consult and cite the final, published document. See http:/www.minsocam.org or GeoscienceWorld

This is the peer-reviewed, final accepted version for American Mineralogist, published by the Mineralogical Society of America.
The published version is subject to change. Cite as Authors (Year) Title. American Mineralogist, in press.
DOI: https://doi.org/10.2138/am-2021-7784. http://www.minsocam.org/

II columnar APDs.

Omphacite in the matrix (MX). MX (Fig. 6f) has abundant equiaxed APDs as well as 3R and 5R. No columnar APDs were observed.

DISCUSSION

Assessment of size distribution patterns of equiaxed APDs

Implications from non-Gaussian size distributions. Temperature dependence of APD coarsening in omphacite was proposed by Carpenter (1981). However, no appropriate method has existed for the quantification of apparent APD-size distribution. Since we cannot explain the multi-modal, non-Gaussian size distributions only based on a single nucleation event of the ordered phase, they must reflect complicated histories of the cation ordering in omphacite. Thus, assessment of the size distributions might enable us to discuss multiple nucleation events of the ordered phase. Although we should also consider some effects of deformation and impurity atoms at APDBs (Ling and Starke 1971; Rase and Mikkola 1975; Carpenter 1979b), the new measurement protocol gives us a key to predicting the cation ordering process at low temperature. In our observations, the mean equiaxed APD size in each of the specimens is quite larger than its major mode by 5–38 nm. Therefore, we cannot rule this out when discussing thermal events during the metamorphism. Moreover, this implies that mean equiaxed APD sizes in omphacite, which are traditionally used for analyses of low-T metamorphic history, are not necessarily appropriate for geothermometry/geospeedometry.

A comparison of garnet-hosted and matrix-forming omphacites. Regarding of

Always consult and cite the final, published document. See http:/www.minsocam.org or GeoscienceWorld

This is the peer-reviewed, final accepted version for American Mineralogist, published by the Mineralogical Society of America.
The published version is subject to change. Cite as Authors (Year) Title. American Mineralogist, in press.
DOI: https://doi.org/10.2138/am-2021-7784. http://www.minsocam.org/

equiaxed APD sizes, we could not confirm any significant difference between garnet-hosted and matrix-forming omphacite. However, we did find that the matrix-forming omphacites (MX and #97647) had lower skewness and kurtosis values compared to the others. Notably, it is crucial that matrix-forming omphacites are likely to have lower kurtosis values; this implies that omphacites in an eclogitic matrix are likely to have wider ranges of APD sizes than omphacite inclusions in garnet. The relatively large APD-size variation in matrix omphacite would be attributed to strong syn- or post-metamorphic deformation effects, because the matrix should have been more subjected to deformation than omphacite inclusions enclosed in their rigid garnet. This tendency indicates that it is reasonable that examining APD sizes of 'omphacite inclusions' will result in a better estimation of its metamorphic *T*–*t* history.

Considering these observations, we need to refine APD-size measurement protocol so that results can be obtained with less arbitrariness. Specifically, it is a crucial problem how we should deal with large and highly distorted APDs. For a better measurement, in essence, we have to interpret the kinetics of APD coarsening appropriately and setting feasible thresholds to get results which make sense for the further discussion and implications.

The origins of columnar APDs

Reassessment of the previously-reported ordering mechanism. We can explain the origins of columnar APDs on the basis of the previous idea that columnar APDs can be formed due to nucleation of the ordered phases at grain boundaries or low angle subgrain boundaries (Lally et al. 1975; Carpenter 1979c). We can envisage a model in which cation ordering occurs at dislocations and/or garnet–omphacite interfaces and, consequently, the APDBs move from those locations.

Always consult and cite the final, published document. See http:/www.minsocam.org or GeoscienceWorld

This is the peer-reviewed, final accepted version for American Mineralogist, published by the Mineralogical Society of America.
The published version is subject to change. Cite as Authors (Year) Title. American Mineralogist, in press.
DOI: https://doi.org/10.2138/am-2021-7784. http://www.minsocam.org/

As we described, however, Type II columnar APDs are less dominant. This is somewhat odd because all of the omphacite inclusions in the garnet have undergone the same metamorphic events, and also the surroundings of the rims of the omphacite inclusions would be similar. If the Type II columnar APDs can be formed merely by cation ordering initiating at garnet–omphacite interfaces due to the excess surface energy, such columnar APDs would be observed more frequently even in the other regions.

The origin of Type II columnar APDs. At the closer side of 3R to the garnet core, the widths of the Type II columnar APDs are highly homogeneous and show a subtle discontinuity of Fe concentration (Fig. 9). This chemical discontinuous feature might indicate that the 3R rim with the Type II columnar APDs formed synchronously when the omphacite was included in the garnet. We interpret this to mean that Type II columnar APDs are common phenomena in syngenetic omphacite inclusions. Generally, omphacite can grow simultaneously with garnet growth in low–*T* eclogite (e.g., Konrad-Schmolke et al. 2008). Our *P*–*T* pseudosection modeling also shows that omphacite with less Fe content is also likely to have grown with the garnet growth (see supplementary Document S2).

Then, the question arises: how can the Type II columnar APDs be formed in syngenetic omphacite? Considering the kinetics of the cation ordering, we propose two possible explanations. One is that the cation ordering occurred preferentially adjacent to preexisting ordered omphacite so that the total surface energy of the antiphase domain boundaries can be smaller. When omphacite grows slightly, the disordered phase firstly appears even though at lower temperature than the ordering temperature of omphacite (e.g., Champness 1973; Carpenter 1978, 1980, 1981; Carpenter and Putnis 1985). If the preferential cation ordering occurred at the

Always consult and cite the final, published document. See http:/www.minsocam.org or GeoscienceWorld

This is the peer-reviewed, final accepted version for American Mineralogist, published by the Mineralogical Society of America.
The published version is subject to change. Cite as Authors (Year) Title. American Mineralogist, in press.
DOI: https://doi.org/10.2138/am-2021-7784. http://www.minsocam.org/

newly formed rim extremely faster than the omphacite growth, bundles of columnar APDs perpendicular to the garnet–omphacite interface are likely to be formed. It might be possible that the ordered phase grew almost epitaxially on the preexisting omphacite rim. In fact, this explanation is reasonable because columnar APDs in alloys can grow simultaneously with their crystallization from melt. For example, Mitsui et al. (1995) interpreted the origins of columnar APDs in Ni_3Al and Cu_3Pt alloys as the migration of grain boundaries of homogeneously ordered crystals. If this interpretation is correct, the widths of such Type II columnar APDs depend on initial equiaxed APD shapes at the preexisting omphacite rim. Therefore, their widths do not necessarily depend only on a growth history of the omphacite rim. In this case, rimward changes of the columnar APD widths would be negligible because newly formed columnar APDs should have the same widths as the preexisting ones.

The alternative explanation is that the ordered phase nucleated in a periodic manner from garnet–omphacite interfaces after the enclosed omphacite finished growing just as the metastable disordered phase. In this case, we cannot dismiss rimward changes of the Type II columnar APD widths. Since the ordered phase nucleates from the interfaces, wider APDs should be observed in closer regions to the omphacite rim. This width variation must reflect the metamorphic history after the omphacite was included in its host garnet.

The most crucial difference between these two possible scenarios is whether the columnar APD widths change rimward or not, but as shown in Figure 5c, this change is difficult to detect. Therefore, we cannot determine which explanation is correct without further information. To further our understanding, more observation is required than that documented in this study.

Always consult and cite the final, published document. See http:/www.minsocam.org or GeoscienceWorld

This is the peer-reviewed, final accepted version for American Mineralogist, published by the Mineralogical Society of America.
The published version is subject to change. Cite as Authors (Year) Title. American Mineralogist, in press.
DOI: https://doi.org/10.2138/am-2021-7784. http://www.minsocam.org/

Heterogeneous distributions of syngenetic omphacite inclusions. If Type II columnar APDs are formed in syngenetic omphacite rims, the question that remains is why we seldom observe such omphacites. When pre-existing omphacites are enclosed in their host garnet, it seems that syn-metamorphic overgrowth does not necessarily occur in all of the omphacite rims. Thus, we discuss below this heterogeneous distribution of syngenetic omphacite rims in the single host garnet by considering its growth history (Fig. 10).

Firstly, a garnet porphyroblast grows slightly to start to enclose an omphacite crystal. At that time, there must be a spatial gap between the garnet and the enclosed omphacite, as inferred from the presence of the fracture-like pores in 4R (e.g., Fig. 6d). Subsequently, if the spatial gap is filled with metamorphic fluids or Ca–Al silicates, the garnet grows slightly to fill the space. If the enclosed omphacite grows synchronously with the garnet growth, the spatial gap should be filled also by the growing omphacite. Note that we can regard the spatial gap as a small closed system wrapped by reaction products; in other words, the major elements for garnet–producing reactions cannot dissipate far away from the spatial gap. Thus, the omphacite can grow more efficiently within the spatial gap than other places as the host garnet grows slightly. Under this assumption, we can postulate a hypothesis that the heterogeneous distribution of syngenetic omphacite rims is attributed to the heterogeneous presence of spatial gaps between the garnet and its omphacite inclusions. If this hypothesis is true, based on the most striking feature that 3R has Type II columnar APDs only on the side closer to the garnet core, we can assume that such small spatial gaps are likely to appear at the closer area to the garnet core. Moreover, this hypothesis might be reasonable because omphacite rims, grown in the spatial gap, are likely to be protected by the garnet from deformation disturbances.

Always consult and cite the final, published document. See http:/www.minsocam.org or GeoscienceWorld

This is the peer-reviewed, final accepted version for American Mineralogist, published by the Mineralogical Society of America.
The published version is subject to change. Cite as Authors (Year) Title. American Mineralogist, in press.
DOI: https://doi.org/10.2138/am-2021-7784. http://www.minsocam.org/

IMPLICATIONS

New constrains on the growth kinetics of garnet-hosted omphacite

Our new finding of syngenetic omphacite with columnar APDs is highly valuable because it would allow us to study the kinetics of the cation ordering in omphacite. Although it is known that nucleation of the disordered phase predates the cation ordering, the kinetics of this process is unclear. Our observation of the periodic columnar APDs must be the very snapshot of growing omphacite with the cation ordering. Considering *P–T–t* information obtained on the basis of geochronology and compositional zoning patterns of garnet, we might be able to understand the initiation of the cation ordering at low temperature.

It is noteworthy that omphacite rims with bundles of columnar APDs would have formed just as they were incorporated into garnet. Over the years, the origins of mineral inclusions, whether they are formed simultaneously with incorporation of them or are remnant fragments of the protolith, are of interest. In the case of sector-zoned garnet, the phenomena that quartz inclusions simultaneously grow with the garnet growth, can be observed (Andersen 1984). Crystallographic orientations of mineral inclusions to their host garnet have been characterized with electron backscatter diffraction in order to estimate their origins (e.g., Griffiths et al. 2016; Ferrero and Angel 2018). However, it remains difficult to know whether a given mineral inclusion was incorporated into its host garnet simultaneously with its growth. Our finding of the heterogeneous distribution of Type II columnar APDs should therefore be a significant contribution to discussing the origins of mineral inclusions. If omphacite with such APDs is a product of reactions producing garnet, analyses of the APD shapes might unravel the timing at which the omphacite was included in the host garnet.

Always consult and cite the final, published document. See http:/www.minsocam.org or GeoscienceWorld

This is the peer-reviewed, final accepted version for American Mineralogist, published by the Mineralogical Society of America.
The published version is subject to change. Cite as Authors (Year) Title. American Mineralogist, in press.
DOI: https://doi.org/10.2138/am-2021-7784. http://www.minsocam.org/

Pitfalls of the APD geospeedometry

Since prograde-zoned garnet itself has a potential to determine *P–T–t* information, we might be able to estimate the garnet growth rate or the timescale of eclogitization by simply applying APD geospeedometry to the omphacite inclusions. However, our FIB–TEM study denies a simple application, because APD-size variation highly reflects a difference in the timings of the nucleation processes of the omphacite. In fact, all of the garnet-rim foils (3R, 4R and 5R) were extracted from the same garnet rim but their equiaxed APD sizes are extremely different. In addition, the presence of Type I columnar APDs means omphacite generally underwent deformation before being enclosed by garnet. To establish more sophisticated geospeedometry based on omphacite APDs, it is critical to focus on omphacite which grew synchronously with the host garnet growth. In other words, understanding of the timing of omphacite incorporation into its host garnet might lead to a refinement of the APD geospeedometry.

Nevertheless, it is not easy to extract temperature/time information only from the Type II columnar APDs because rimward changes of their shapes are small. Therefore, future work should be directed towards analyzing more omphacite inclusions within a single prograde-zoned garnet, understanding the critical trends of columnar APD shapes, and modeling their growths. This is important not only for understanding the kinetics of the cation ordering in omphacite but also for unraveling the kinetics of low–*T* eclogitization in subduction zones.

CONCLUSION

We studied five omphacite inclusions in a garnet from Syros eclogite by FIB–TEM technique capable of site-specific extraction of inclusions using a scanning electron beam. We found

Always consult and cite the final, published document. See http:/www.minsocam.org or GeoscienceWorld

This is the peer-reviewed, final accepted version for American Mineralogist, published by the Mineralogical Society of America.
The published version is subject to change. Cite as Authors (Year) Title. American Mineralogist, in press.
DOI: https://doi.org/10.2138/am-2021-7784. http://www.minsocam.org/

abundant equiaxed and dislocation-related columnar APDs. In addition, we found bundles of columnar APDs aligned perpendicular to garnet–omphacite interfaces and concluded that this texture can be formed simultaneously with host-garnet growth. Further analysis of these peculiar textures may lead to an understanding of the kinetics of the cation ordering in omphacite and low–*T* eclogitization.

ACKNOWLEDGEMENTS

This research was supported by CNEAS at Tohoku University, BGI at the University of Bayreuth, and the University of Tokyo, and was funded in part by grants from the MEXT/JSPS KAKENHI JP18H01299 to TT and the ERI JURP 2018-B-01 to TT and RF. The authors acknowledge the International Joint Graduate Program in Earth and Environmental Sciences (GP-EES) and the JSPS Japanese–German Graduate Externship. The Scios FIB and the Titan G2 TEM at BGI were financed by DFG grant Nos. INST 91/315-1 FUGG and INST 91/251-1 FUGG, respectively. We appreciate for the reviews of our research that were received from two anonymous reviewers. We also thank Bradley De Gregorio for constructive editorial evaluation.

Always consult and cite the final, published document. See http:/www.minsocam.org or GeoscienceWorld

This is the peer-reviewed, final accepted version for American Mineralogist, published by the Mineralogical Society of America.
The published version is subject to change. Cite as Authors (Year) Title. American Mineralogist, in press.
DOI: https://doi.org/10.2138/am-2021-7784. http://www.minsocam.org/

REFERENCES CITED

Abràmoff, M.D., Magalhães, P.J., and Ram, S.J. (2004) Image processing with imageJ. Biophotonics International, 11, 36−42.

Andersen, T.B. (1984) Inclusion patterns in zoned garnets from Magerøy, north Norway. Mineralogical Magazine, 48, 21–26.

Arganda-Carreras, I., Kaynig, V., Rueden, C., Eliceiri, K.W., Schindelin, J., Cardona, A., and Seung, H.S. (2017) Trainable Weka Segmentation: a machine learning tool for microscopy pixel classification. Bioinformatics, 33, 2424−2426.

Brenker, F.E., Müller, W.F., and Brey, G.P. (2003) Variation of antiphase domain size in omphacite: A tool to determine the temperature–time history of eclogites revisited. American Mineralogist, 88, 1300–1311.

Carpenter, M.A. (1978) Kinetic control of ordering and exsolution in omphacite. Contributions to Mineralogy and Petrology, 67, 17–24.

Carpenter, M.A. (1979a) Omphacites from Greece, Turkey, and Guatemala: composition limits of cation ordering. American Mineralogist, 64, 102–108.

Carpenter, M.A. (1979b) Experimental coarsening of antiphase domains in a silicate mineral. Science, 206, 681–683.

Carpenter, M.A. (1979c) Contrasting properties and behaviour of antiphase domains in pyroxenes. Physics and Chemistry of Minerals, 5, 119–131.

Carpenter, M.A. (1980) Mechanism of exolution in sodic pyroxene. Contributions to Mineralogy and Petrology, 71, 289–300.

Always consult and cite the final, published document. See http:/www.minsocam.org or GeoscienceWorld

This is the peer-reviewed, final accepted version for American Mineralogist, published by the Mineralogical Society of America.
The published version is subject to change. Cite as Authors (Year) Title. American Mineralogist, in press.
DOI: https://doi.org/10.2138/am-2021-7784. http://www.minsocam.org/

Carpenter, M.A. (1981) Omphacite microstructures as time-temperature Indicators of blueschist- and eclogite-facies metamorphism. Contributions to Mineralogy and Petrology, 78, 441–451.

Carpenter, M.A., and Putnis, A. (1985) Cation order and disorder during crystal growth: some implications for natural mineral assemblages. In A.B. Thompson, and D.C. Rubie, Ed., Metamorphic Reactions, p. 1–26. Springer, New York.

Champness, P.E. (1973) Speculation on an order-disorder transformation in omphacite. American Mineralogist, 58, 540–542.

Clark, J.R., Appleman, D.E., and Papike, J.J. (1969) Crystal-chemical characterization of clinopyroxene based on eight new structure refinements. Mineralogical Society of America Special Paper, 2, 31–50.

Ferrero, S., and Angel, R.J. (2018) Micropetrology: Are Inclusions Grains of Truth? Journal of Petrology, 59, 1671−1700.

Fukushima, R., Tsujimori, T., Aoki, S., and Aoki, K. (in revision) Trace-element zoning patterns in porphyroblastic garnet in low-*T* eclogite: Parameter optimization of the diffusion-limited REE-uptake model. Island Arc.

García-Casco, A., Vega, A.R., Párraga, J.C., Iturralde-Vinent, M.A., Lázaro, C., Quintero, I.B., Agramonte, Y.R., Kröner, A., Cambra, K.N., Millán, G., Torres-Roldán, R.L., and Carrasquilla, S. (2009) A new jadeitite jade locality (Sierra del Convento, Cuba): first report and some petrological and archeological implications. Contributions to Mineralogy and Petrology, 158, 1–16.

Always consult and cite the final, published document. See http:/www.minsocam.org or GeoscienceWorld

This is the peer-reviewed, final accepted version for American Mineralogist, published by the Mineralogical Society of America.
The published version is subject to change. Cite as Authors (Year) Title. American Mineralogist, in press.
DOI: https://doi.org/10.2138/am-2021-7784. http://www.minsocam.org/

Griffiths, T.A., Habler, G., and Abart, R. (2016) Crystallographic orientation relationships in host–inclusion systems: new insights from large EBSD data sets. American Mineralogist, 101, 690–705.

Joanes, D.N., and Gill, C.A. (1998) Comparing measures of sample skewness and kurtosis. The Statistician, 47, 183–189.

Konrad-Schmolke, M., O'Brien, P.J., de Capitani, C., and Carswell, D.A. (2008) Garnet growth at high- and ultra-high pressure conditions and the effect of element fractionation on mineral modes and composition. Lithos, 103, 309–332.

Lagos, M., Scherer, E.E., Tomaschek, F., Münker, C., Keiter, M., Berndt, J., and Ballhaus, C. (2007) High precision Lu–Hf geochronology of Eocene eclogite-facies rocks from Syros, Cyclades, Greece. Chemical Geology, 243, 16–35.

Lally, J.S., Heuer, A.H., Nord, G.L. Jr., and Christie, J.M. (1975) Subsolidus reactions in lunar pyroxenes: an electron petrographic study. Contributions to Mineralogy and Petrology, 51, 263–281.

Laurent, V., Lanari, P., Naïr, I., Augier, R., Lahfid, A., and Jolivet, L. (2018) Exhumation of eclogite and blueschist (Cyclades, Greece): Pressure–temperature evolution determined by thermobarometry and garnet equilibrium modeling. Journal of Metamorphic Geology, 36, 769–798.

Ling, F.W., and Starke, E.A. Jr. (1971) The development of long-range order and the resulting strengthening effects in Ni_4Mo. Acta Metallurgica, 19, 759–768.

Lister, G.S., and Forster, M.A. (2016) White mica $^{40}Ar/^{39}Ar$ age spectra and the timing of multiple episodes of high-P metamorphic mineral growth in the Cycladic eclogite–

Always consult and cite the final, published document. See http:/www.minsocam.org or GeoscienceWorld

This is the peer-reviewed, final accepted version for American Mineralogist, published by the Mineralogical Society of America.
The published version is subject to change. Cite as Authors (Year) Title. American Mineralogist, in press.
DOI: https://doi.org/10.2138/am-2021-7784. http://www.minsocam.org/

blueschist belt, Syros, Aegean Sea, Greece. Journal of Metamorphic Geology, 34, 401–421.

Matsumoto, T., and Banno, S. (1970) A natural pyroxene with space group C^4_{2h} = P2/n. Proceedings of the Japan Academy, 46, 173–175.

Mitsui, K., Suzuki, T., and Mishima, Y. (1995) Anti-phase domain morphology and its formation process in melt-quenched Ni_3Al. Intermetallics, 3, 161–166.

Rase, C.L., and Mikkora, D.E. (1975) Effect of excess Au on antiphase domain growth in Cu_3Au. Metallurgical and Materials Transactions A, 6, 2267–2271.

Schindelin, J., Arganda-Carreras, I., Frise, E., Kaynig, V., Longair, M., Pietzsch, T., Preibisch, S., Rueden, C., Saalfeld, S., Schmid, B., Tinevez, J.Y., White, D.J., Hartenstein, V., Eliceiri, K., Tomancak, P., and Cardona, A. (2012) Fiji: an open-source platform for biological-image analysis. Nature Methods, 9, 676−682.

Schumacher, J.C., Brady, J.B., Cheney, J.T., and Tonnsen, R.R. (2008) Glaucophane-bearing marbles on Syros, Greece. Journal of Petrology, 49, 1667–1686.

Seck, H.A., Kötz, J., Okrusch, M., Seidel, E., and Stosch, H.G. (1996) Geochemistry of a meta-ophiolite suite: an association of metagabbros, eclogites and glaucophanites on the island of Syros, Greece. European Journal of Mineralogy, 8, 607–623.

Takahashi, N., Tsujimori, T., Kayama, M., and Nishido, H. (2017) Cathodoluminescence petrography of P–type jadeitites from the New Idria serpentinite body, California. Journal of Mineralogical and Petrological Sciences, 112, 291–299.

Tomaschek, F., Kennedy, A.K., Villa, L.M., Lagos, M., and Ballhaus, C. (2003) Zircons from Syros, Cyclades, Greece — recrystallization and mobilization of zircon during high-pressure metamorphism. Journal of Petrology, 44, 1977–2002.

Always consult and cite the final, published document. See http:/www.minsocam.org or GeoscienceWorld

This is the peer-reviewed, final accepted version for American Mineralogist, published by the Mineralogical Society of America.
The published version is subject to change. Cite as Authors (Year) Title. American Mineralogist, in press.
DOI: https://doi.org/10.2138/am-2021-7784. http://www.minsocam.org/

Tsujimori, T. (1997) Omphacite-diopside vein in an omphacitite block from the Osayama serpentinite melange, Sangun-Renge metamorphic belt, southwestern Japan. Mineralogical Magazine, 61, 845–852.

Tsujimori, T., and Liou, J.G. (2004) Coexisting chromian omphacite and diopside in tremolite schist from the Chugoku Mountains, SW Japan: The effect of Cr on the omphacite-diopside immiscibility gap. American Mineralogist, 89, 7–14.

Tsujimori, T., and Mattinson, C. (2020) Eclogites in different tectonic settings. In S. Elias, and D. Alderton, Ed., Encyclopedia of Geology, 2nd Edition. Elsevier. doi:10.1016/B978-0-08-102908-4.00104-1.

Tsujimori, T., Liou, J.G., and Coleman, R.G. (2005) Coexisting retrograde jadeite and omphacite in a jadeite-bearing lawsonite eclogite from the Motagua Fault Zone, Guatemala. American Mineralogist, 90, 836–842.

Uunk, B., Brouwer, F., ter Voorde, M., and Wijbrans, J. (2018) Understanding phengite argon closure using single grain fusion age distributions in the Cycladic Blueschist Unit on Syros, Greece. Earth and Planetary Science Letters, 484, 192–203.

Van Roemund, H.L.M., and Lardeaux, J.M. (1991) Modification of antiphase domain sizes in omphacite by dislocation glide and creep mechanisms and its petrological consequences. Mineralogical Magazine, 55, 397–407.

Warner, J. (1964) X-ray crystallography of omphacite. American Mineralogist, 49, 1461–1467.

Yokoyama, K., Banno, S., and Matsumoto, T. (1976) Compositional range of *P*2/*n* omphacite from the eclogitic rocks of central Shikoku, Japan. Mineralogical Magazine, 40, 773–779.

Always consult and cite the final, published document. See http:/www.minsocam.org or GeoscienceWorld

This is the peer-reviewed, final accepted version for American Mineralogist, published by the Mineralogical Society of America.
The published version is subject to change. Cite as Authors (Year) Title. American Mineralogist, in press.
DOI: https://doi.org/10.2138/am-2021-7784. http://www.minsocam.org/

FIGURE CAPTIONS

Figure 1. Images of the investigated garnet: **a** BSE image; **b** X-ray map of Mg/(Mg + Fe) (intensity ratio); **c** X-ray map of Ca; **d** X-ray map of Mn. The subscript i after each element symbol indicates that the image was obtained based solely on the signal intensity. Locations from which we extracted omphacite thin foils are also shown: (i) 1C, (ii) 2M, (iii) 3R, (iv) 4R, and (v) 5R. The white circle in the BSE image indicates the location of the garnet core estimated based on its euhedral outline and major-element zoning patterns.

Figure 2. Representative line profiles of Mn (solid line) and Y (dashed line) in the investigated garnet. They represent kernel regression lines based on the measured data (Fukushima et al. in revision). Band widths are set to 27% for both. The region of the mantle (gray) is defined as 30–85% of the total radius. Approximate locations of the investigated omphacites are also shown.

Figure 3. Locations from which we obtained omphacite thin foils are indicated by the white rectangles. The black arrows indicate the directions to the center of the garnet core.

Figure 4. TEM images of 1C including garnet–omphacite interfaces: **a** dark-field image (g = 050) of equiaxed/Type II columnar APDs and the inset selected area electron diffraction pattern (Z = [001]); **b** dark-field image (g = 050) of Type I columnar APDs. The white arrows in **a** indicate Type II columnar APDs. Grt = garnet, Omp = omphacite.

Always consult and cite the final, published document. See http:/www.minsocam.org or GeoscienceWorld

This is the peer-reviewed, final accepted version for American Mineralogist, published by the Mineralogical Society of America.
The published version is subject to change. Cite as Authors (Year) Title. American Mineralogist, in press.
DOI: https://doi.org/10.2138/am-2021-7784. http://www.minsocam.org/

Figure 5. TEM images of 2M (**a**) and 3R (**b** and **c**): **a** dark-field image of 2M ($g = \bar{1}40$) including a garnet–omphacite interface; **b** dark-field image of 3R (g = 050) including a garnet–omphacite interface closer to the garnet rim; **c** dark-field image of 3R (g = 050) including the other garnet–omphacite interface closer to the garnet core. At the bottom of **c**, columnar APDs are aligned perpendicular to the garnet–omphacite interface (Type II columnar APDs).

Figure 6. TEM images of 4R (**a**–**d**), 5R (**e**) and MX (**f**): **a, b** dark-field images of 4R (g = 050) including abundant Type I columnar APDs; **c** dark-field image of 4R (g = 050) including a garnet–omphacite interface and equiaxed APDs; **d** bright field image ($g = 0\bar{5}0$) of the same area as **c**; **e** dark-field image of 5R (g = 050) including a garnet–omphacite boundary; **f** dark-field image of MX (g = 050).

Figure 7. Histograms of measured APD sizes in **a** 1C, **b** 3R, **c** 4R, and **d** 5R. As insets, we show binarized dark-field images from which noise and highly distorted APDs are excluded. Results of the kernel density estimates are also shown. Band widths of the density estimates are: 8.303 nm (1C), 12.93 nm (3R), 3.214 nm (4R) and 17.07 nm (5R). For each of the diagrams, the black and gray triangles indicate its mode and mean values, respectively.

Figure 8. Results of APD-size measurement in matrix-forming omphacites (**a, b** MX; **c, d** sample #97647 in Carpenter (1978)). Binarized images of dark-field TEM images are shown in the left side, while histograms of measured APD sizes and the kernel density estimates are shown in the right side. As insets, we also show binarized images after noise and highly distorted APDs

Always consult and cite the final, published document. See http:/www.minsocam.org or GeoscienceWorld

This is the peer-reviewed, final accepted version for American Mineralogist, published by the Mineralogical Society of America.
The published version is subject to change. Cite as Authors (Year) Title. American Mineralogist, in press.
DOI: https://doi.org/10.2138/am-2021-7784. http://www.minsocam.org/

are excluded. Band widths of the density estimates are 16.54 nm (MX) and 6.031 nm (#97647). The black and gray triangles indicate the mode and mean values, respectively.

Figure 9. Scanning TEM images of the Type II columnar APDs in 3R: **a** bright-field image; **b, c, d** X-ray maps of Na, Ca and Fe, respectively. The black arrows in **a** indicate the Type II columnar APDs. We added a white dashed line to **c** in order to emphasize the garnet–omphacite interface.

Figure 10. Schematic diagram showing our hypothesis to explain the heterogeneous distribution of syngenetic omphacites in a single host garnet.

Always consult and cite the final, published document. See http:/www.minsocam.org or GeoscienceWorld

This is the peer-reviewed, final accepted version for American Mineralogist, published by the Mineralogical Society of America.
The published version is subject to change. Cite as Authors (Year) Title. American Mineralogist, in press.
DOI: https://doi.org/10.2138/am-2021-7784. http://www.minsocam.org/

Fukushima et al., **Figure 1.** [1-page width]

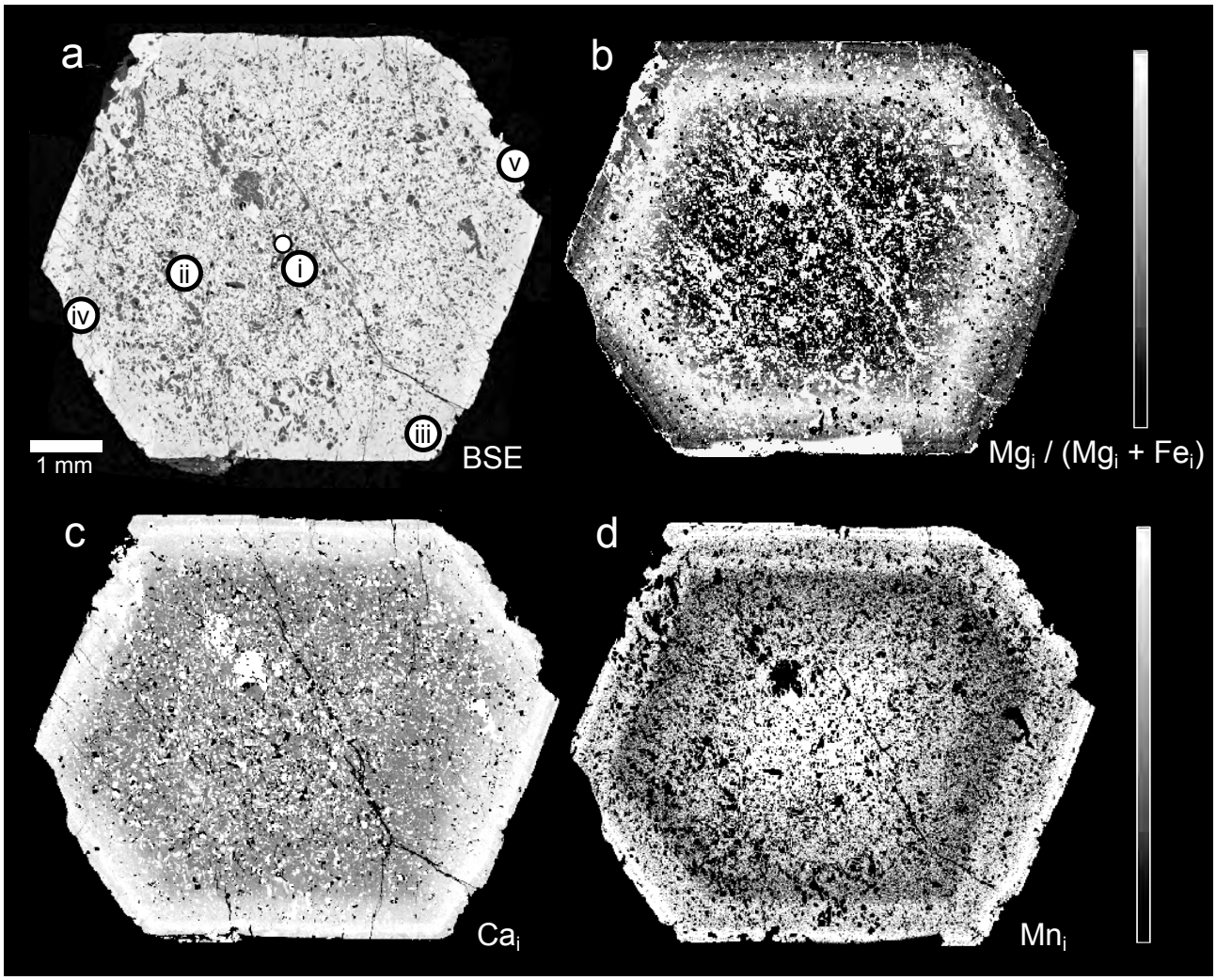

Always consult and cite the final, published document. See http:/www.minsocam.org or GeoscienceWorld

This is the peer-reviewed, final accepted version for American Mineralogist, published by the Mineralogical Society of America.
The published version is subject to change. Cite as Authors (Year) Title. American Mineralogist, in press.
DOI: https://doi.org/10.2138/am-2021-7784. http://www.minsocam.org/

Fukushima et al., **Figure 2.** [1-column width]

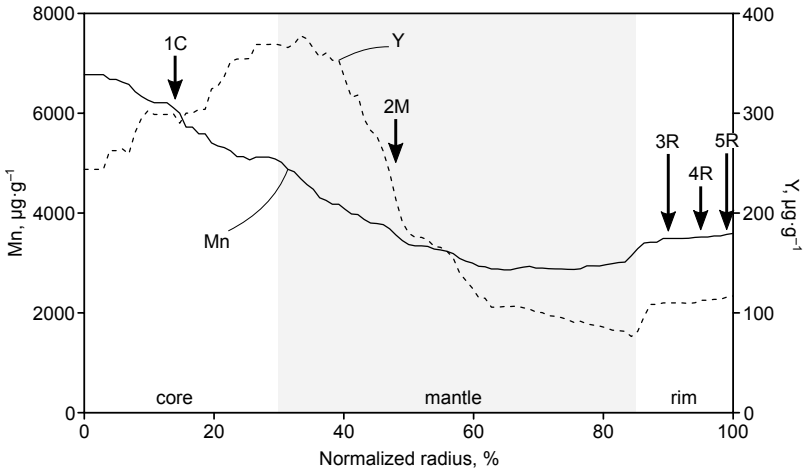

Always consult and cite the final, published document. See http:/www.minsocam.org or GeoscienceWorld

This is the peer-reviewed, final accepted version for American Mineralogist, published by the Mineralogical Society of America.
The published version is subject to change. Cite as Authors (Year) Title. American Mineralogist, in press.
DOI: https://doi.org/10.2138/am-2021-7784. http://www.minsocam.org/

Fukushima et al., **Figure 3.** [1-page width]

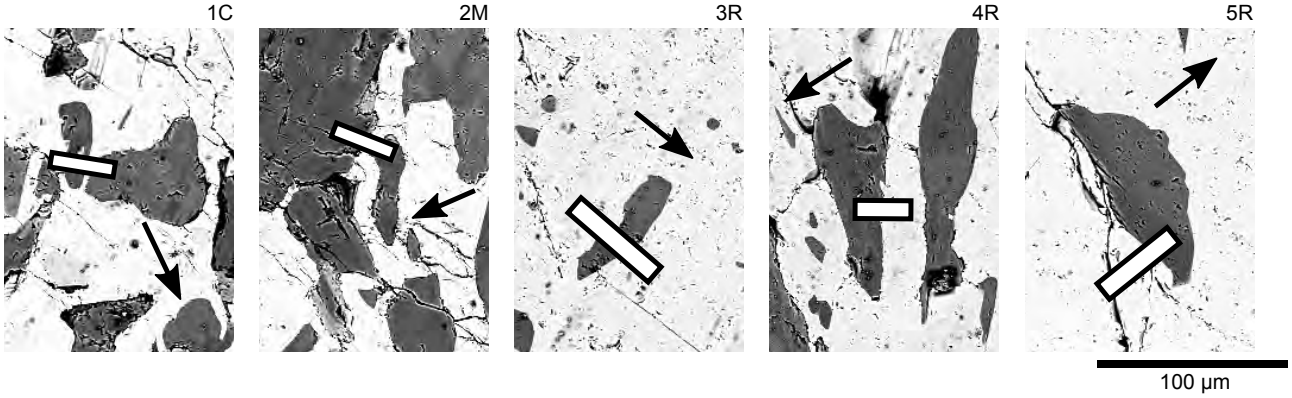

Always consult and cite the final, published document. See http:/www.minsocam.org or GeoscienceWorld

This is the peer-reviewed, final accepted version for American Mineralogist, published by the Mineralogical Society of America.
The published version is subject to change. Cite as Authors (Year) Title. American Mineralogist, in press.
DOI: https://doi.org/10.2138/am-2021-7784. http://www.minsocam.org/

Fukushima et al., **Figure 4.** [1-column width]

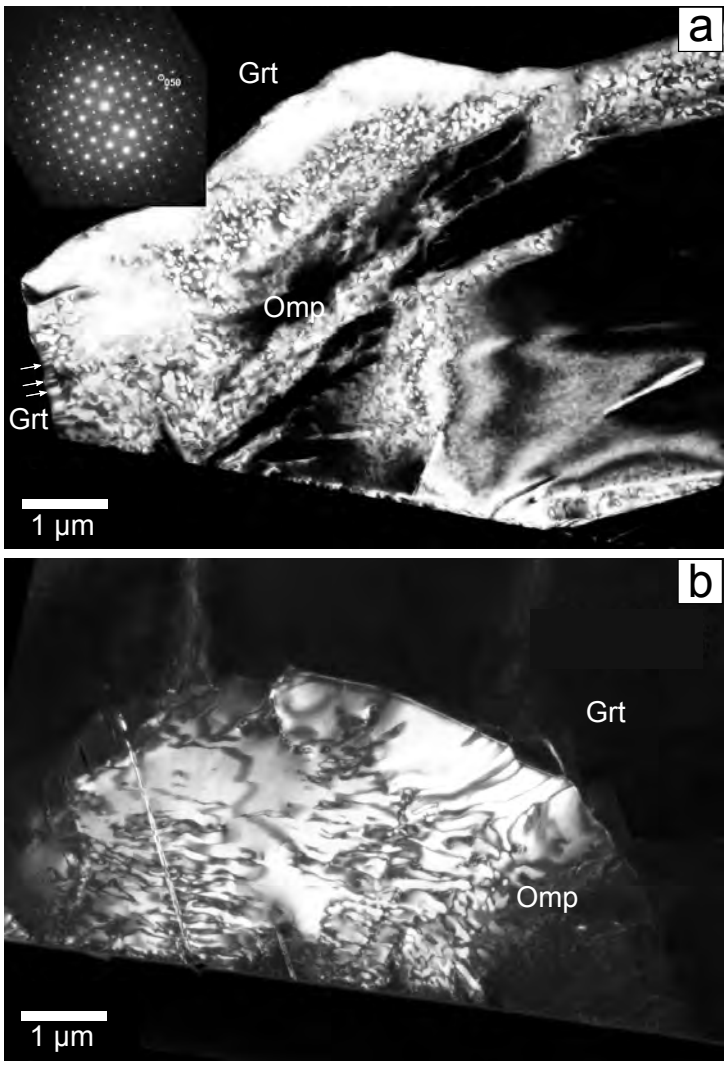

Always consult and cite the final, published document. See http:/www.minsocam.org or GeoscienceWorld

This is the peer-reviewed, final accepted version for American Mineralogist, published by the Mineralogical Society of America.
The published version is subject to change. Cite as Authors (Year) Title. American Mineralogist, in press.
DOI: https://doi.org/10.2138/am-2021-7784. http://www.minsocam.org/

Fukushima et al., **Figure 5.** [1-page width]

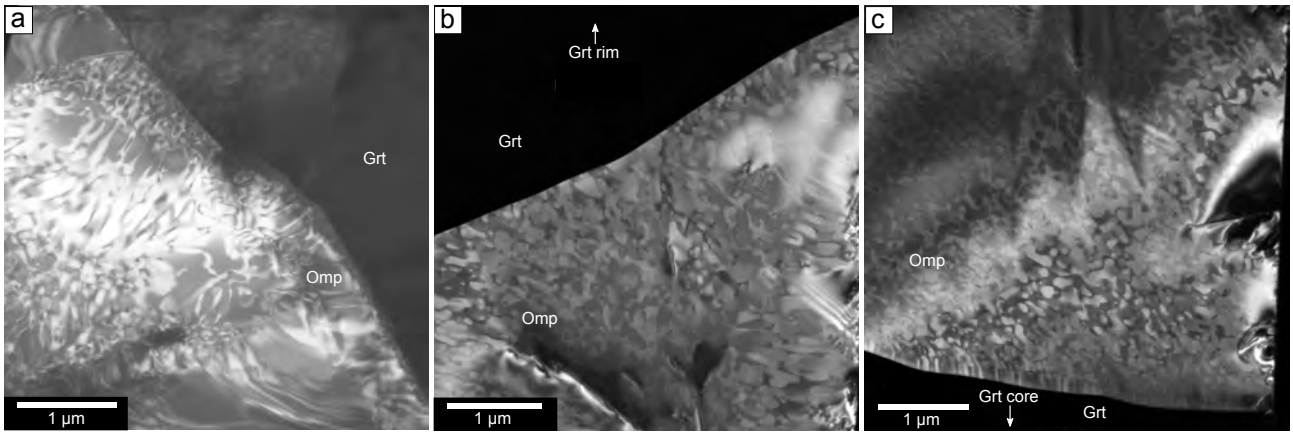

Always consult and cite the final, published document. See http:/www.minsocam.org or GeoscienceWorld

This is the peer-reviewed, final accepted version for American Mineralogist, published by the Mineralogical Society of America.
The published version is subject to change. Cite as Authors (Year) Title. American Mineralogist, in press.
DOI: https://doi.org/10.2138/am-2021-7784. http://www.minsocam.org/

Fukushima et al., **Figure 6.** [1-page width]

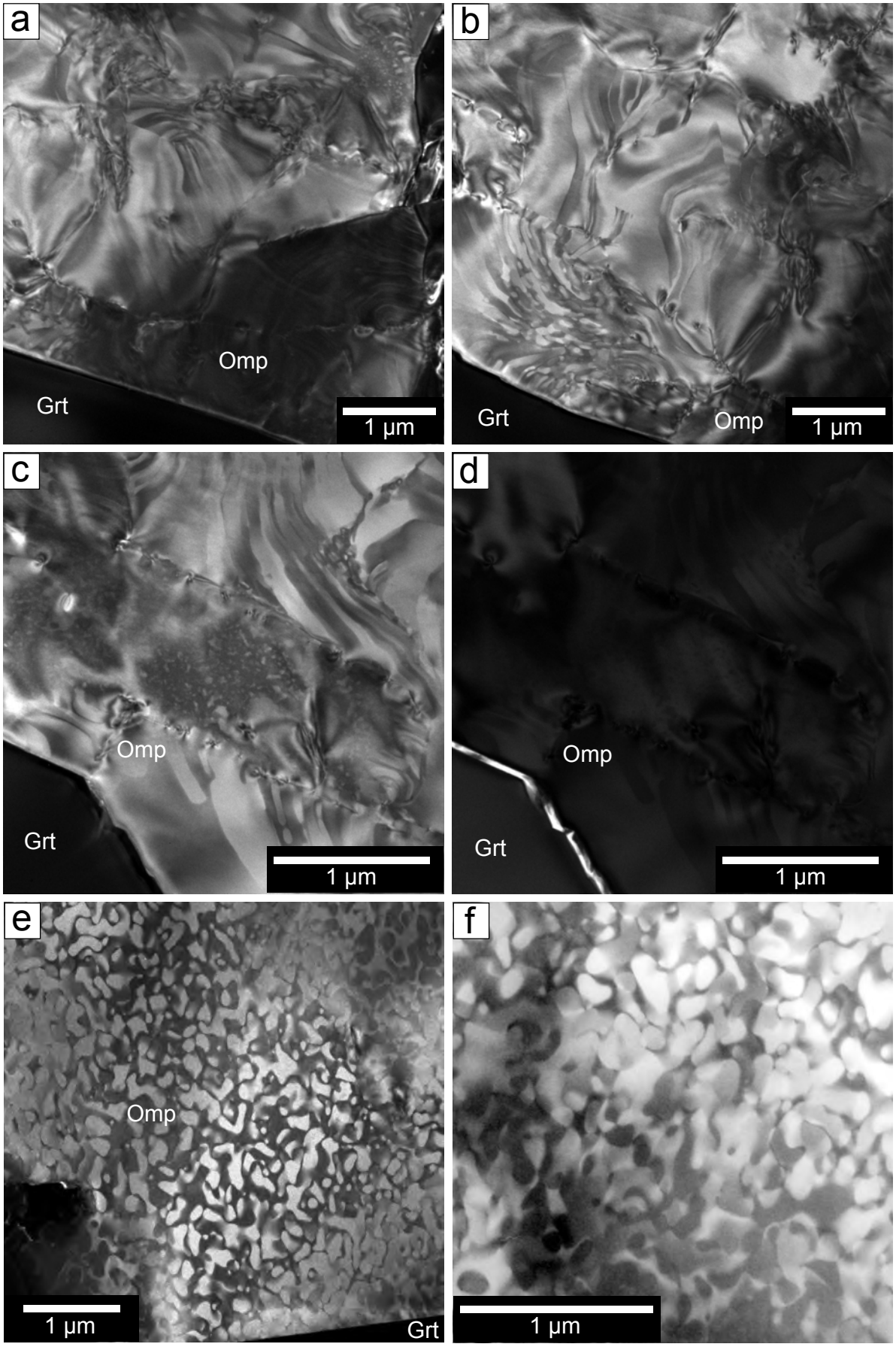

Always consult and cite the final, published document. See http:/www.minsocam.org or GeoscienceWorld

This is the peer-reviewed, final accepted version for American Mineralogist, published by the Mineralogical Society of America.
The published version is subject to change. Cite as Authors (Year) Title. American Mineralogist, in press.
DOI: https://doi.org/10.2138/am-2021-7784. http://www.minsocam.org/

Fukushima et al. **Figure 7.** [1-page width]

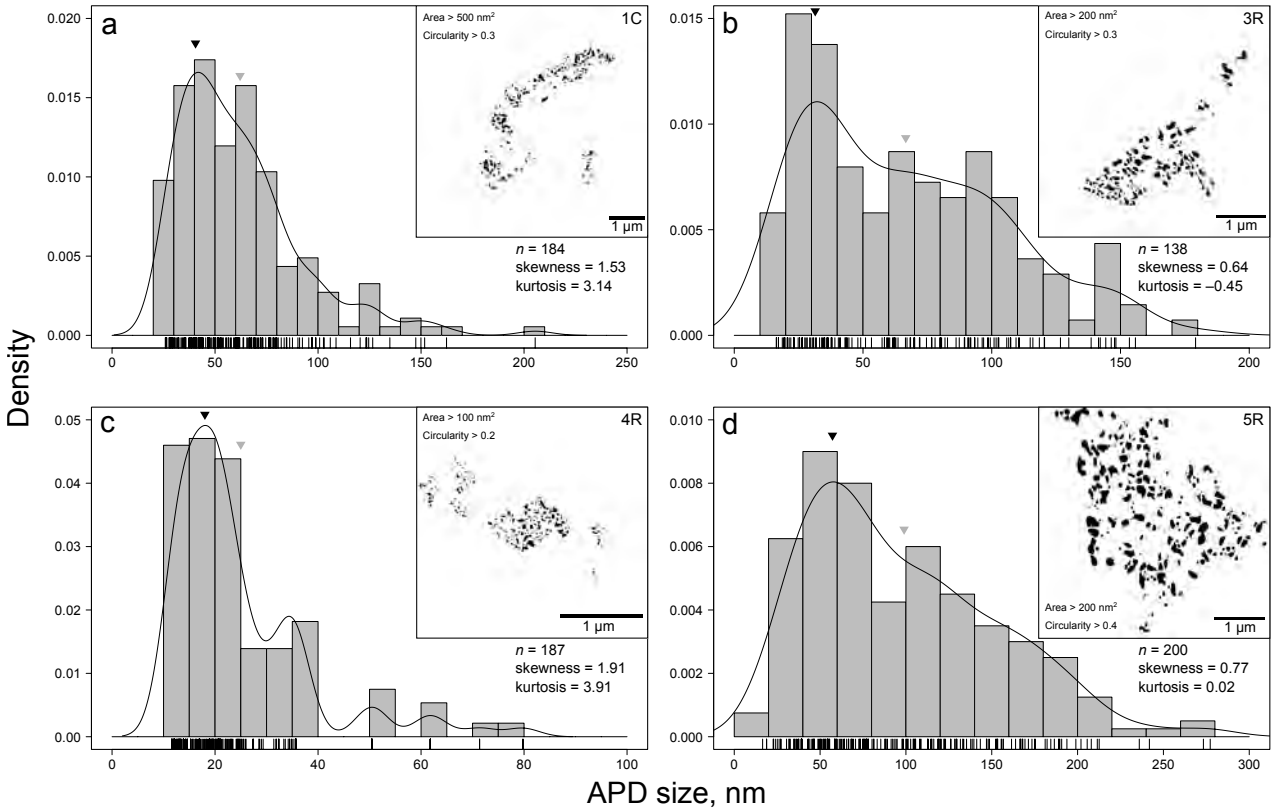

Always consult and cite the final, published document. See http:/www.minsocam.org or GeoscienceWorld

This is the peer-reviewed, final accepted version for American Mineralogist, published by the Mineralogical Society of America.
The published version is subject to change. Cite as Authors (Year) Title. American Mineralogist, in press.
DOI: https://doi.org/10.2138/am-2021-7784. http://www.minsocam.org/

Fukushima et al. **Figure 8.** [1-page width]

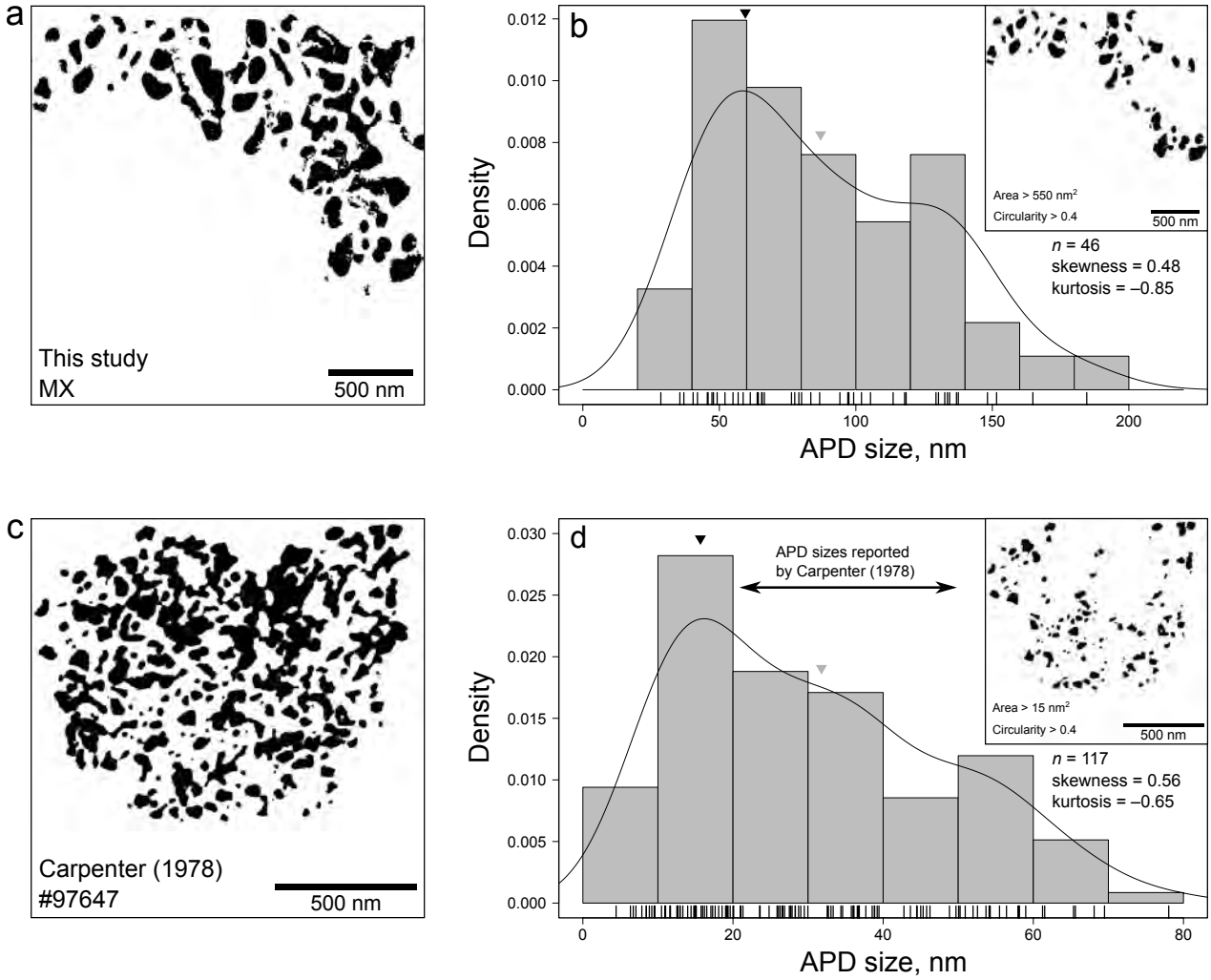

Always consult and cite the final, published document. See http:/www.minsocam.org or GeoscienceWorld

This is the peer-reviewed, final accepted version for American Mineralogist, published by the Mineralogical Society of America.
The published version is subject to change. Cite as Authors (Year) Title. American Mineralogist, in press.
DOI: https://doi.org/10.2138/am-2021-7784. http://www.minsocam.org/

Fukushima et al. **Figure 9.** [1-page width]

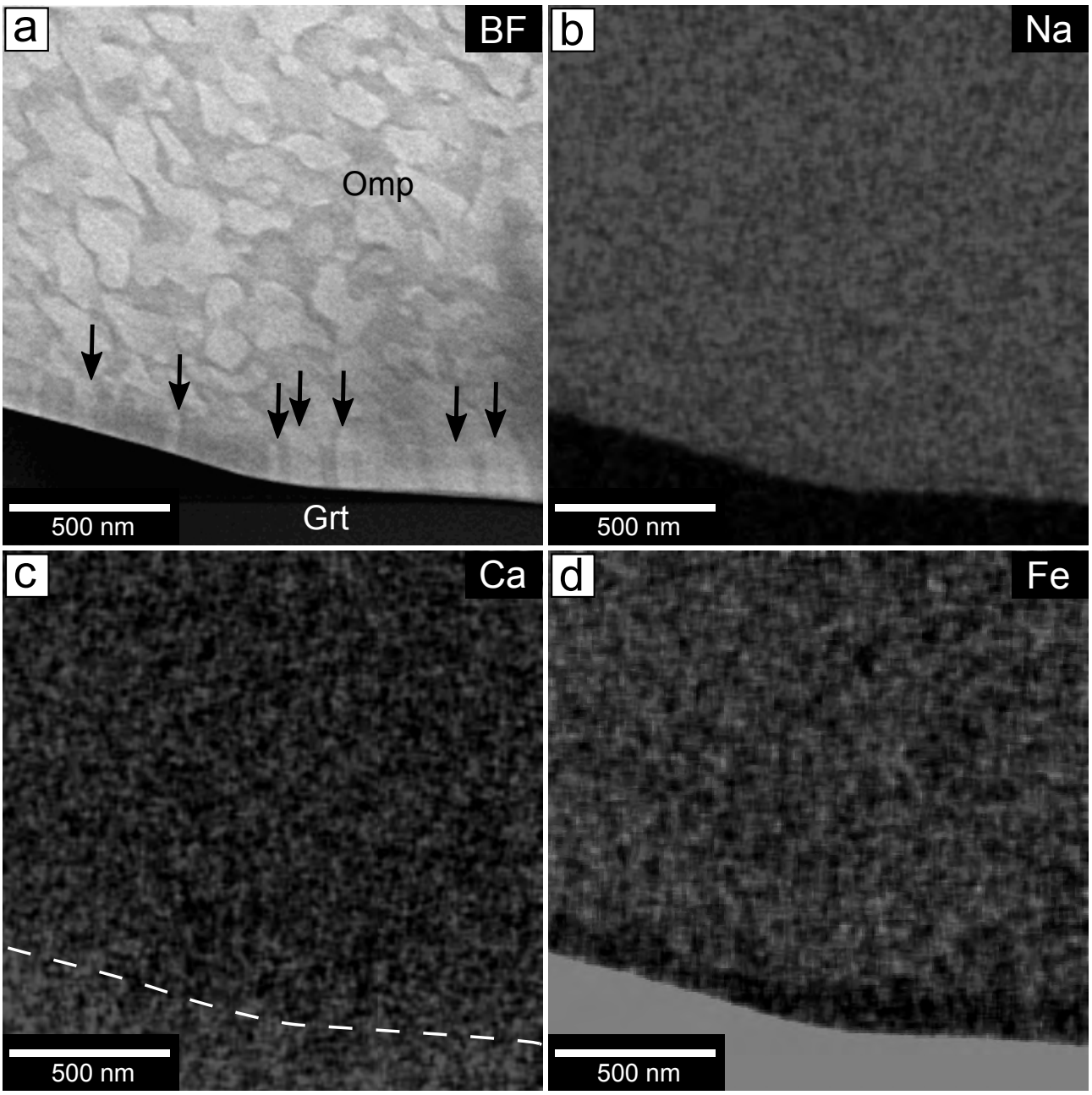

Always consult and cite the final, published document. See http:/www.minsocam.org or GeoscienceWorld

This is the peer-reviewed, final accepted version for American Mineralogist, published by the Mineralogical Society of America.
The published version is subject to change. Cite as Authors (Year) Title. American Mineralogist, in press.
DOI: https://doi.org/10.2138/am-2021-7784. http://www.minsocam.org/

Fukushima et al. **Figure 10.** [1-page width]

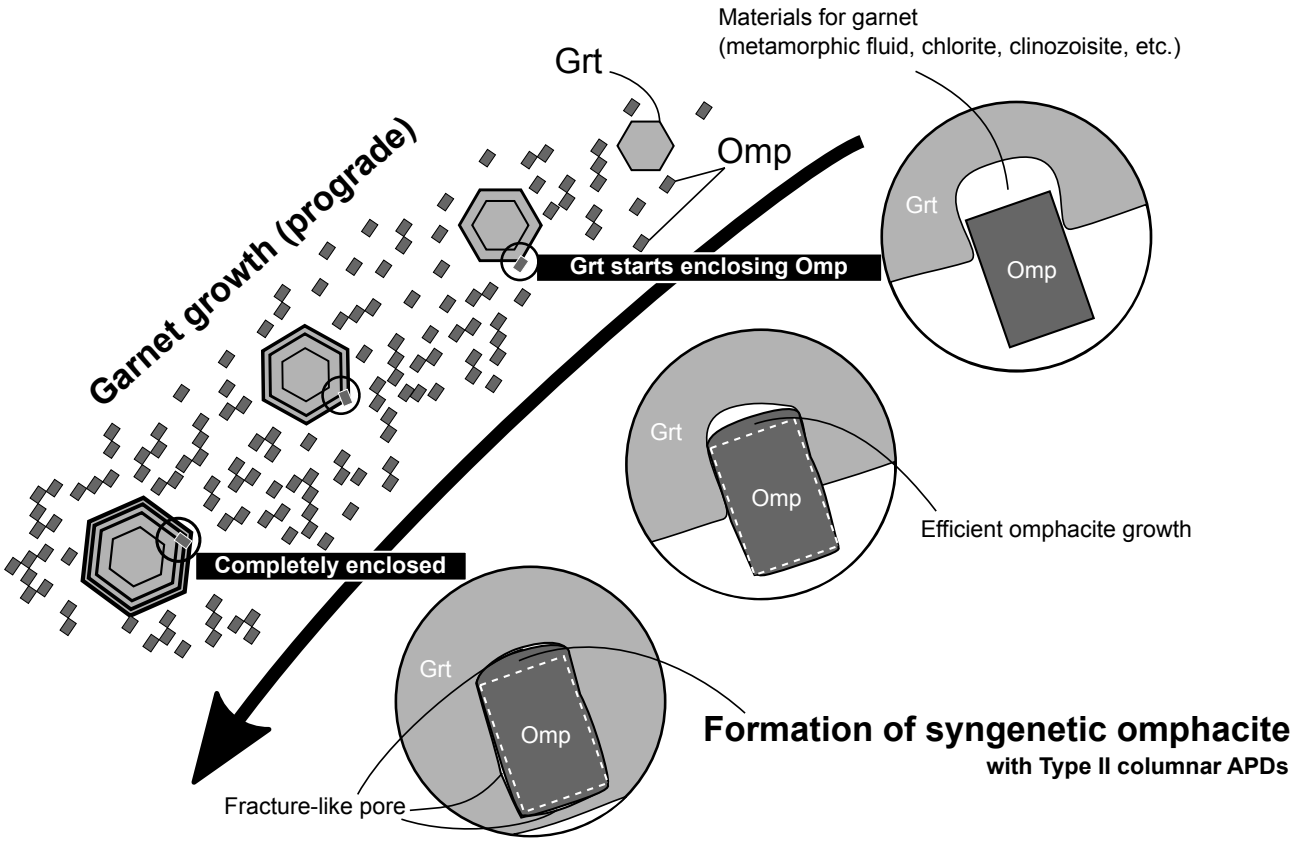

Always consult and cite the final, published document. See http:/www.minsocam.org or GeoscienceWorld